Quantifying the impact of cell-to-cell inconsistency on electric vehicle battery degradation and utilization

Citation for the original published paper (version of record):
Zhou, L., Bian, X., Zhang, Y. et al (2026). Quantifying the impact of cell-to-cell inconsistency on electric vehicle battery degradation
and utilization. Nature Energy: 1-11. http://dx.doi.org/10.1038/s41560-026-02131-5

nature energy

Analysis

https://doi.org/10.1038/s41560-026-02131-5

Quantifying the impact of cell-to-cell inconsistency on electric vehicle battery degradation and utilization

Received: 9 June 2025

Accepted: 29 July 2026

Published online: 25 August 2026

Check for updates

Litao Zhou[1,2,3,4,5,7], Xiaolei Bian[3,7], Yizhou Zhang[3,6], Zhenpo Wang[4,5], Zhongwei Chen[1,2], Zhiyu Mao[1,2] & Changfu Zou[3]

Enhancing utilization rates of battery systems in electric vehicles (EVs) substantially benefits economic efficiency and environmental sustainability. However, cell-to-cell inconsistency remains a critical barrier to fully realizing these advantages, and its system-level impact under real-world EV operation is still poorly quantified. Here we present a dataset containing 116 passenger cars and 17 buses, encompassing operational data spanning more than 3 years and up to 300,000 km per vehicle. Using practical measurements, we estimate individual cell capacity and resistance and construct a diagnostic framework of six metrics capturing variability in cell health, pack capacity retention, lifetime degradation, state-of-charge utilization, power capability and energy utilization. Our analysis reveals substantial performance degradation, including battery health reductions of 6.2% for passenger cars and 7.5% for buses, lifetime shortening by 17.7% and 22.8% and power capability decreases of 12.9% and 15.1%, respectively. Consequently, energy-resource utilization is limited to 80.7% for cars and 72.9% for buses over their operational lifespans. These findings underscore the necessity of consistency control for advancing EV battery technologies.

The integration of hundreds or thousands of cells in electric vehicle (EV) battery packs makes cell-to-cell inconsistency a critical concern as it can reduce overall utilization and substantially shorten pack lifetime[1]. This heterogeneity can arise from multiple sources. Differences in raw-material quality, manufacturing variability and improper cell grouping can give rise to cell-to-cell variation even before battery use[2,3]. In more severe cases, insufficient quality control may allow cells with latent defects into battery packs, precipitating premature failure and further increasing inconsistency. During operation, cells degrade at different rates, primarily owing to temperature differences associated with cell position and cooling-system layout[4]. Mechanical stress and vibration can also differentially affect cell internal structure and electrochemical behaviour[5]. Cell inconsistency is therefore ubiquitous across battery systems: even under well-regulated and otherwise identical laboratory conditions, cells can follow markedly different ageing trajectories[6–8].

Cell inconsistency impairs pack-level performance because faster-ageing cells develop lower capacity or higher internal resistance than their counterparts, becoming bottlenecks within the pack[9]. During charging, the lowest-capacity cell reaches the upper voltage limit first, prematurely terminating charging of the series-connected pack[10]. Similarly, the cell with the highest internal resistance constrains power output, whereas the most severely aged cell ultimately determines pack lifetime[11]. Relative to an ideal pack with uniform cell performance,

[1]Power Battery and System Research Centre, Dalian Institute of Chemical Physics, Chinese Academy of Sciences, Dalian, China. [2]State Key Laboratory of Catalysis, Dalian Institute of Chemical Physics, Chinese Academy of Sciences, Dalian, China. [3]Department of Electrical Engineering, Chalmers University of Technology, Gothenburg, Sweden. [4]National Engineering Research Center for Electric Vehicles, Beijing Institute of Technology, Beijing, China. [5]School of Mechanical Engineering, Beijing Institute of Technology, Beijing, China. [6]Zeekr Technology Europe AB, Gothenburg, Sweden. [7]These authors contributed equally: Litao Zhou, Xiaolei Bian. e-mail: zwchen@dicp.ac.cn; changfu.zou@chalmers.se

 https://doi.org/10.1038/s41560-026-02131-5

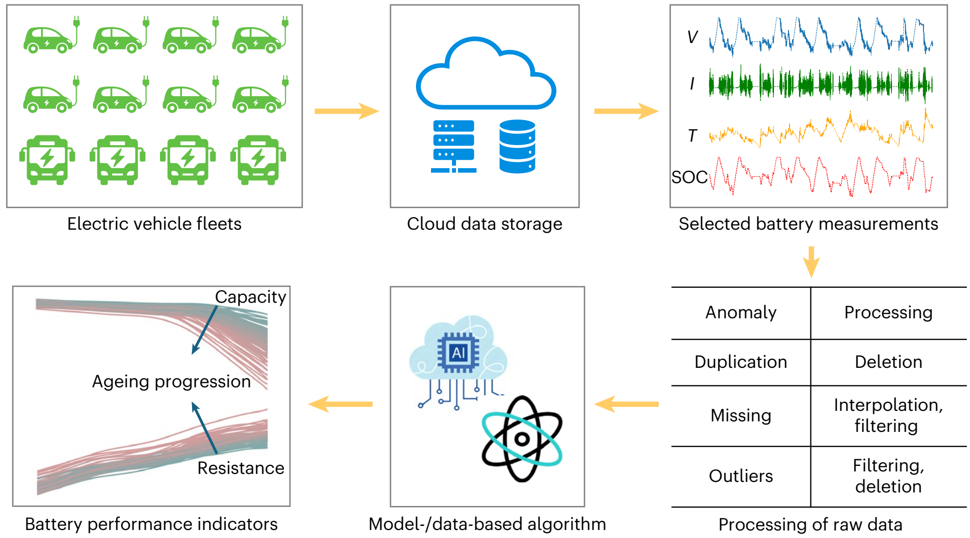

Fig. 1 | EV fleet data generation and preprocessing workflow. Operational signals were collected from EV fleets via electronic control units and BMSs and transmitted to a cloud-based data centre. Battery measurements and states (voltage (*V*), current (*I*), SOC and temperature (*T*)) were curated for analysis. Preprocessing addressed data issues such as anomalies, missing values, duplications and outliers through deletion, interpolation and filtering. Event detection (for example, slow charging events spanning wide SOC windows) enabled approximate calibration of battery capacity. The resulting dataset provides a foundation for analysing cell-to-cell heterogeneity, ageing behaviour and degradation evolution across large EV fleets. Credit: electric vehicle icons, Noun Project.

these bottlenecks reduce capacity utilization, limit available power and shorten operational lifetimes, thereby diminishing the economic and environmental benefits of EVs.

Considerable efforts have been made to evaluate and mitigate cell inconsistency. Existing inconsistency metrics commonly use cell-level signals such as voltage, current, temperature, capacity and resistance[12–14]. Among these, voltage is the most widely used measurement owing to its ease of acquisition[1,15,16]. Such inconsistencies have been assessed using statistical analysis[17], clustering algorithms[15,18], machine learning techniques[3] and information fusion strategies[2,19]. Although valuable, these studies have generally been limited to small-scale datasets or laboratory settings. To mitigate inconsistency, state-of-the-art battery management systems (BMSs) seek to limit cell-to-cell divergence through state-of-charge (SOC) balancing and thermal management[20–24]. However, the long-term, system-level consequences of cell-to-cell inconsistency have not been comprehensively quantified in large-scale real-world EV fleets.

In this study, we develop a fleet-scale framework to quantify how cell-to-cell inconsistency constrains the long-term performance of real-world EV battery packs. Using routinely recorded voltage, current and temperature measurements, we estimate and harmonize cell-level capacity and resistance trajectories for 116 passenger cars equipped with nickel–manganese–cobalt (NMC) batteries, monitored over more than three years, with individual vehicles accumulating up to 300,000 km; 17 electric buses equipped with lithium-iron-phosphate (LFP) batteries serve as a complementary reference. Across the two fleets, cell inconsistency reduces usable pack-level state of health (SOH) by 6.2% and 7.5%, shortens pack lifetime by 17.7% and 22.8% relative to the average lifetime of the constituent cells and reduces power capability by 12.9% and 15.1%, respectively. Consequently, passenger car and bus packs realize only 80.7% and 72.9%, respectively, of their available energy resources before retirement.

Real-world EV fleet dataset

To investigate large-scale real-world battery usage patterns in EVs, we utilized a fleet dataset sourced from the National Monitoring and Management Centre for New Energy Vehicles. The data generation and preprocessing workflow is illustrated in Fig. 1. Key parameters, including vehicle speed, accumulated mileage, battery pack and cell voltages, currents, temperatures, insulation resistance, fault alarms and the operational states of motors, motor controllers and braking systems, were recorded in real time by onboard electronic control units and BMSs. These measurements were transmitted wirelessly at a nominal frequency of 0.1 Hz, aggregated within a cloud-based data centre, enabling centralized storage, monitoring, visualization and analysis. The data items, formats and communication protocols adhered to the national standard specified in ref. 25 and have been described in detail in ref. 26. From the raw dataset, we curated the battery signals most relevant to this study, namely pack-level voltage and current, cell-level SOC, cell voltage and temperature. The resulting processed dataset contains 587.5 million data rows, covering 116 electric cars and 17 electric buses, with individual vehicle mileages reaching up to 300,000 km. The fleet includes both NMC and LFP batteries in prismatic cell configurations, which dominate the current EV market. This large-scale dataset enables quantification of long-term cell-level ageing and performance heterogeneity in real-world EV battery systems. Further details on the dataset and BMS functionalities, battery-system specifications and dataset characteristics are provided in Supplementary Note 1, Supplementary Table 1 and Supplementary Figs. 1–4, respectively.

EV fleet datasets are often affected by data integrity issues arising from sensor malfunctions, intermittent communication and storage errors, which pose substantial challenges to extracting reliable ageing insights. Therefore, the first stage of preprocessing focused on systematically identifying and removing discontinuous, duplicated or incomplete data series segments to ensure temporal consistency and signal reliability. A further challenge in fleet-scale datasets is the absence of labelled ground truth outputs, such as battery capacity measured under standardized conditions, which are essential for ageing quantification. To address this limitation, we developed practical calibration strategies (Methods). In particular, data samples from slow, long-duration charging events characterized by low current rates and wide SOC windows were used to approximately calibrate battery capacity. Accordingly, the second stage of preprocessing involved detecting such charging events and extracting the corresponding data segments. To enable consistent analysis across vehicles and degradation stages, we further excluded vehicles with an initial mileage

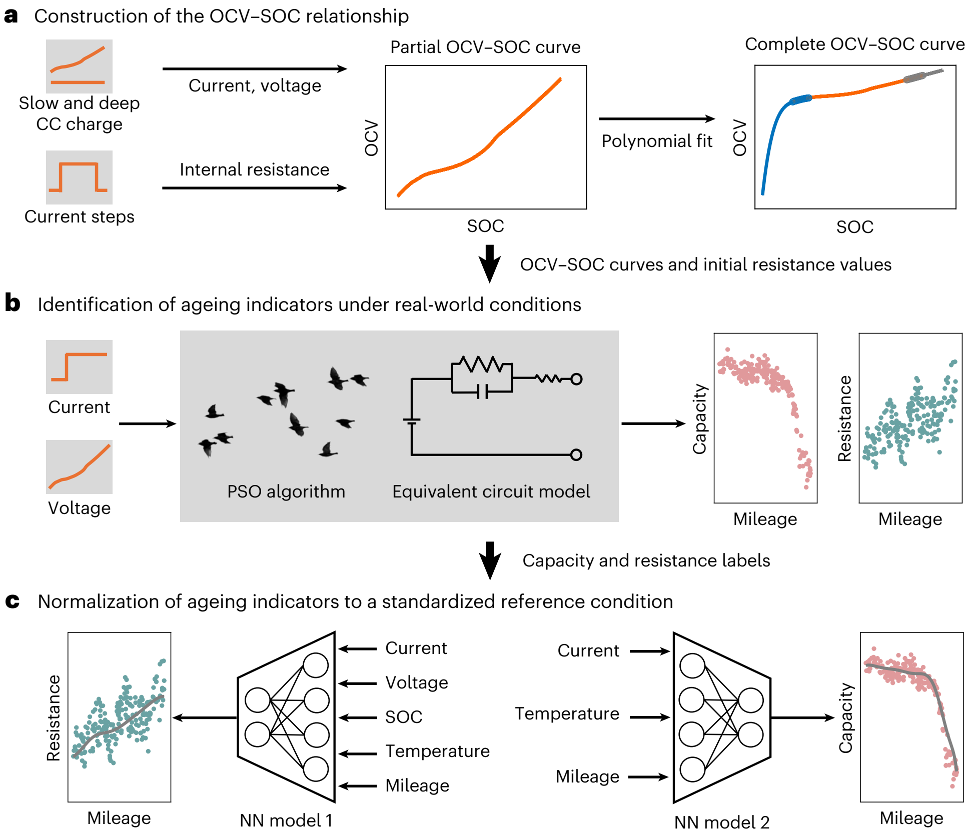

Fig. 2 | Identification and normalization of battery ageing indicators from real-world EV fleet data. a, Construction of the OCV–SOC relationship. The orange curve in the right panel represents the partial OCV–SOC profile obtained from direct measurements after removing the ohmic drop. Blue and grey curves denote extrapolated profiles at the low- and high-SOC regions based on transitional points marked by blue and grey circles, respectively. **b**, PSO-based parameter identification using an equivalent circuit model to estimate cell ageing indicators under real-world operational conditions. **c**, Normalization of cell ageing indicators to a standardized reference condition using deep neural networks. The normalized indicators are represented by grey curves. CC, constant current; PSO, particle swarm optimization; NN, neural network.

exceeding 100,000 kilometres and vehicles with insufficient accumulated mileage for reliable ageing characterization. This multi-stage preprocessing pipeline ensures a high-quality dataset that captures the temporal evolution and heterogeneity of battery degradation, thereby establishing a robust foundation for fleet-scale ageing and performance analyses. The results of each data cleaning step are summarized in Supplementary Fig. 5.

Normalized cell ageing trajectories

The dynamic performance, driving range, charging behaviour and reliability of an EV are strongly governed by the properties of its battery pack, including capacity, power capability and energy throughput. These properties evolve over time and, in the long term, can be characterized by the capacity and internal (ohmic) resistance of the pack and its constituent cells[27]. Accordingly, evaluating system-level ageing requires continuous and accurate tracking of cell-level capacity fade and power fade, commonly quantified as SOH with respect to capacity and internal resistance, respectively.

Due to manufacturing variability and non-uniform usage conditions, cells within the same battery pack inevitably age at different rates. To quantify this cell-to-cell ageing heterogeneity in real-world EV fleets and assess its long-term implications for system performance, we develop a framework to estimate the capacity and resistance trajectories of individual cells, as summarized in Fig. 2. This framework comprises three steps: (1) establishing the relationship between open-circuit voltage (OCV) and SOC for the cells; (2) estimating cell capacity and resistance under real-world operational conditions and (3) harmonizing these estimates by projecting them onto a standardized reference condition.

In real-world EV fleets, although many studies have reported promising results for battery health estimation[28,29], most treat the battery pack as an aggregated unit when quantifying the levels of energy, power and health. This aggregation can oversimplify, and in some cases effectively mask, the temporal evolution of cell-level disparities. Moreover, battery ageing in practical EV operation is governed by complex and interdependent factors, such as current, temperature, SOC and mileage. These interactions pose a substantial challenge for consistent characterization and comparison of battery ageing under real-world operation[30,31]. To address this challenge, harmonized cell-level ageing indicators are used to reduce the influence of heterogeneous operational factors and enable meaningful comparison of degradation evolution across cells and EV battery systems, as detailed in the Methods.

Pack performance constrained by cell heterogeneity

Ageing characteristics of EV battery packs

To investigate the ageing characteristics of EV battery cells, Fig. 3 presents the measured voltage signals, estimated health indicators and their harmonized degradation trajectories for a representative electric passenger car equipped with an NMC battery pack. Cell capacities are normalized to the nominal capacity of new cells, and the resulting values are referred to as capacity-defined SOH.

At early stages of operation, the charging voltage profiles of all 95 cells in the pack (Fig. 3a) exhibit a high degree of uniformity. Even in

https://doi.org/10.1038/s41560-026-02131-5

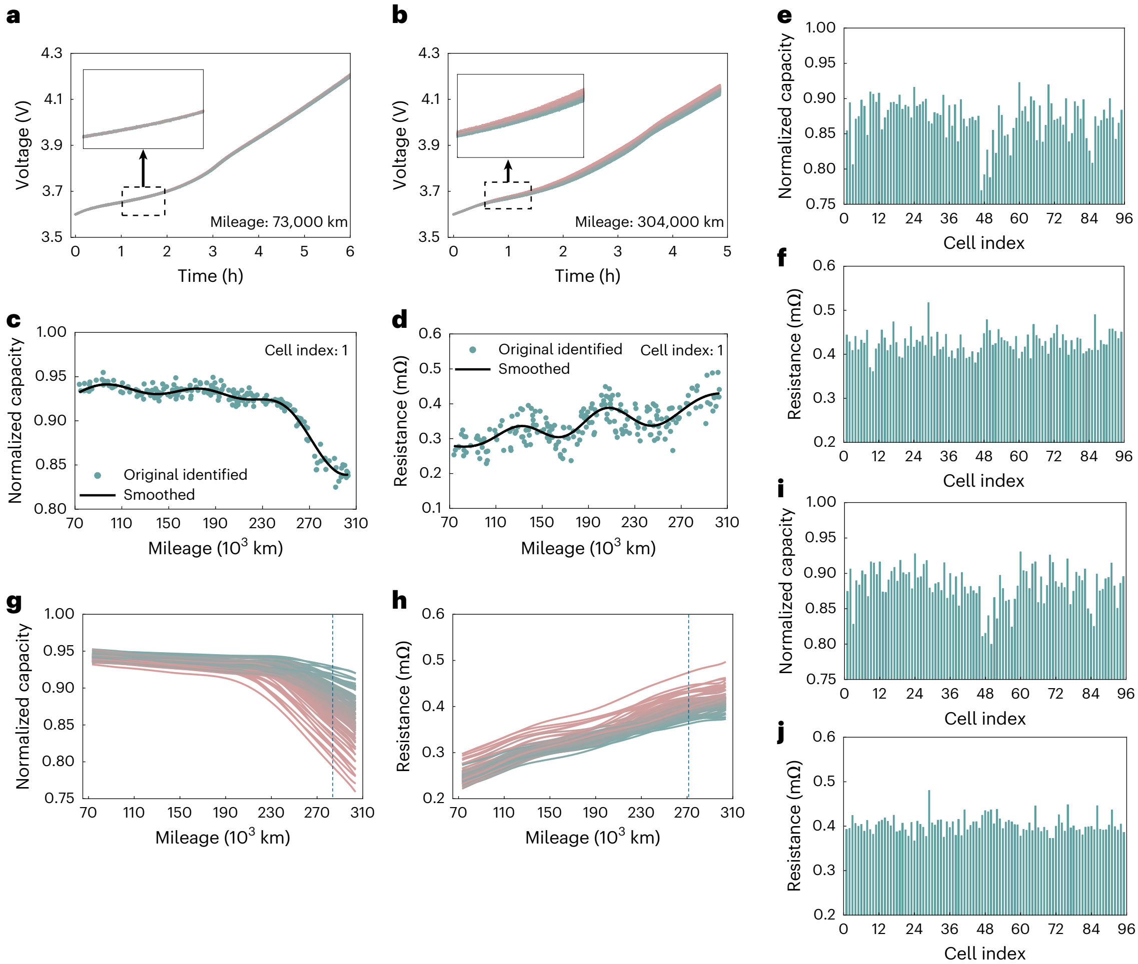

Fig. 3 | Inhomogeneous ageing of NMC battery cells in an electric passenger car. a,**b**, Cell charging voltage profiles at accumulated mileages of 73,000 km (**a**) and 304,000 km (**b**), respectively. **c**,**d**, Normalized capacity (**c**) and resistance estimates (**d**) for Cell 1 under real-world operational conditions. Black curves denote smoothed trajectories obtained using support vector regression. **e**,**f**, Cell-wise normalized capacity (**e**) and resistance estimates (**f**) under real-world operational conditions at an accumulated mileage of 280,000 km. **g**,**h**, Harmonized ageing trajectories of all 95 cells in the battery pack after projection to a standardized reference condition. The vertical dashed lines indicate an accumulated mileage of 280,000 km. Coloured curves are used to distinguish overlapping individual cell trajectories. **i**,**j**, Corresponding cell-wise normalized capacity (**i**) and resistance estimates (**j**) projected to the reference condition at 280,000 km.

the zoomed-in inset, cell-to-cell variations are virtually indistinguishable. However, as the battery ages, pronounced voltage divergence emerges among the cells, despite identical charging conditions. For example, at an accumulated mileage of 304,000 km (Fig. 3b), the voltage spread becomes particularly evident at high-SOC levels. This widening imbalance reflects a progressive loss of electrochemical uniformity within the pack and raises a fundamental question: how can such heterogeneous electrical signatures be harnessed to track cell-specific ageing evolution?

As shown in Fig. 3c,d, the cell capacities decrease while the resistance values generally increase as mileage accumulates, leading to shortened driving range and reduced power capability for the EV. Notably, the health indicators estimated under real-world operational conditions do not evolve monotonically with mileage. For instance, the resistance profile of a representative cell (Cell 1, Fig. 3d) exhibits periodic upward fluctuations superimposed on a long-term rising trend. Similarly, the cell capacity profile during the early mileage range displays multiple local maxima (Fig. 3c). These fluctuations are primarily driven by operational and environmental variations, most notably temperature. Seasonal effects are evident: resistance tends to peak in colder months and drop during warmer periods, consistent with known temperature-dependent electrochemical behaviour[32,33]. For the capacity profile of the demonstrated EV cell, a distinct 'knee' point appears beyond 240,000 km, marking the onset of accelerated degradation.

The ageing of EV battery packs is governed by a complex interplay of factors, such as current rates, voltage thresholds, SOC windows, temperature conditions and total mileage. However, the stochastic nature of real-world usage combined with spatial environmental heterogeneity across cells makes direct comparison of the initially estimated health indicators (Fig. 3c,d) problematic. Such comparisons can obscure underlying degradation patterns and lead to inaccurate or biased conclusions. To address this challenge, we develop deep neural-network models to quantify the relationships between each ageing indicator and its associated stress factors (Methods). By projecting all cells onto a standardized reference condition (for example, a common temperature of 27 °C), the ageing trajectories of capacity and resistance are harmonized across the EV battery pack (Fig. 3g,h). The resulting profiles show monotonic capacity decay and resistance growth with mileage, while revealing substantial variation in the rate and magnitude of degradation across cells. These disparities progressively widen over time and reach their peak near the end of life.

To provide a fleet-level overview, Fig. 4 and Supplementary Fig. 6 show the distributions of normalized capacity and resistance at early and late stages of ageing for 12 passenger cars equipped with NMC

https://doi.org/10.1038/s41560-026-02131-5

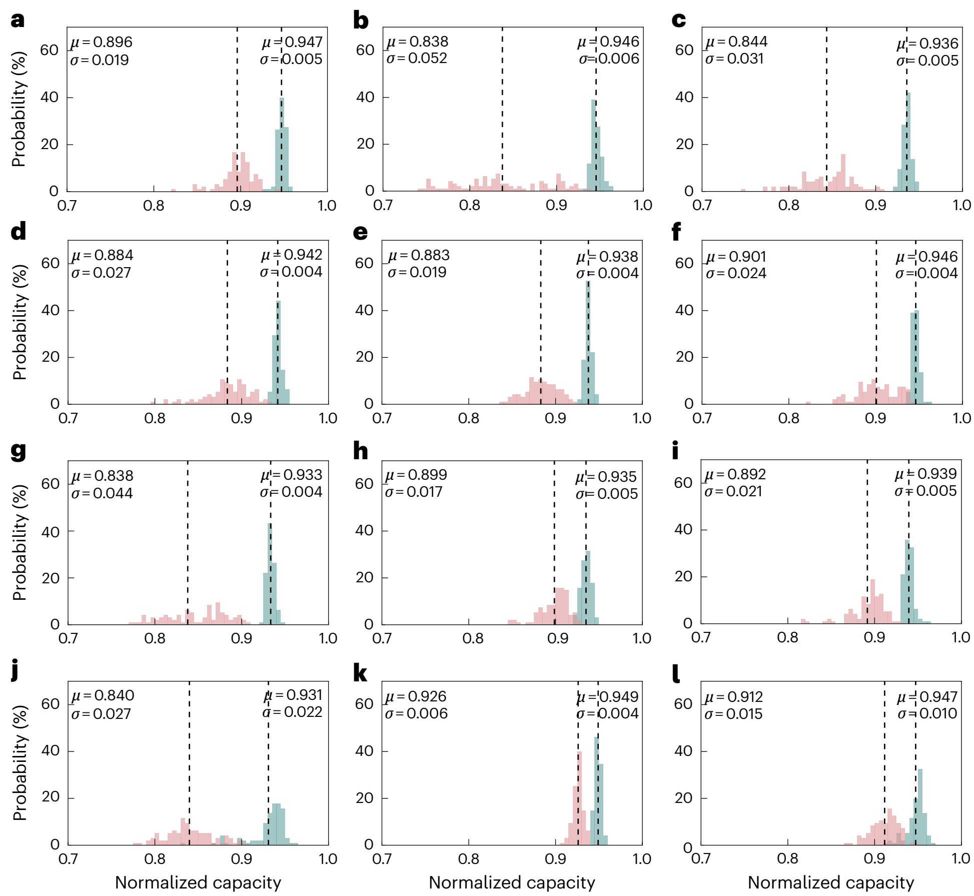

Fig. 4 | Histograms of normalized capacity distributions at early and late ageing stages for 12 passenger cars equipped with NMC batteries. Early ageing stage is 80,000 km, 27 °C (blue) and late ageing stage is 280,000 km, 27 °C (pink). **a**–**l**, Each panel corresponds to a different vehicle, showing the mean (μ) and standard deviation (σ) values for the normalized capacity distributions. Vertical dashed lines indicate the mean capacity values, illustrating the progression of degradation from early to late stages.

batteries. As shown in Fig. 4, the normalized capacity distribution shifts from a higher mean and smaller standard deviations during the early stages (blue) to a lower mean with increased dispersion at later stages (pink). This shift indicates progressive battery degradation, that is, the decreased capacity and increased cell-to-cell variation. The internal resistance exhibits an analogous ageing trend, where distributions move towards higher resistance values as batteries age (Supplementary Fig. 6). Collectively, these distributional shifts indicate both the progression of ageing and the concurrent amplification of heterogeneity within battery packs over their operational lifetimes.

Inconsistency as the limiting factor in pack performance

Cell-to-cell inconsistency within EV battery systems, particularly in internal resistance and capacity, can markedly degrade system-level performance, including driving range, power capability and lifetime. These performance metrics are typically constrained by the weakest-performing cells. To quantify how cell inconsistency affects real-world battery-system performance, we define six metrics (Methods include detailed definitions): σ_{SOH} quantifies the dispersion in SOH across individual cells; β_{SOH} measures the overall impact of cell inconsistency on pack SOH; β_{life} evaluates the utilization rate of battery lifetime; β_{SOC} assesses the impact of inconsistency on usable capacity; β_{power} quantifies the influence of resistance heterogeneity on power capability and β_{energy} captures the overall lifetime utilization rate of battery energy resources, as constrained by cell inconsistency.

The standard deviation of SOH across all cells within a battery pack, σ_{SOH}, directly reflects cell inconsistency. Figure 5a shows the evolution of σ_{SOH} for 19 EVs equipped with NMC batteries over approximately 300,000 km. Up to 170,000 km, SOH dispersion remains low across the fleet. Beyond this mileage, many vehicles exhibit a pronounced increase in inconsistency due to accelerated ageing of specific cells approaching their degradation thresholds ('ageing knees'), consistent with Fig. 3g. This behaviour is most plausibly associated with cells that have less favourable initial conditions or harsher local operating histories, such as higher local temperature exposure, larger voltage excursions or stronger current-induced stress, which cause them to reach accelerated ageing regimes earlier than other cells in the same pack. At the fleet level, substantial variability is observed even among vehicles of the same model: the worst-performing vehicle (dark red curve) shows a sharp rise in SOH dispersion around 170,000 km, whereas the best-performing vehicles (blue curves) maintain minimal dispersion up to 300,000 km. This heterogeneity highlights the importance of continuous long-term monitoring to accurately assess both pack-level and cell-level ageing trajectories. The evolution of σ_{SOH} across the vehicle fleet is not necessarily monotonic, as illustrated by several examples in Fig. 5a. This behaviour reflects nonlinear and time-varying ageing dynamics of battery cells within each vehicle.

Cell inconsistency adversely impacts overall battery pack SOH, as pack performance is limited by the weakest cells. The parameter β_{SOH}, defined as the ratio of the minimum cell SOH to the average SOH of all cells in the pack, quantifies this impact. Figure 5b shows that β_{SOH} remains relatively stable for all vehicles up to approximately 170,000 km, after which many vehicles show a noticeable decline due to accelerated degradation of their weakest cells. This trend aligns closely with

https://doi.org/10.1038/s41560-026-02131-5

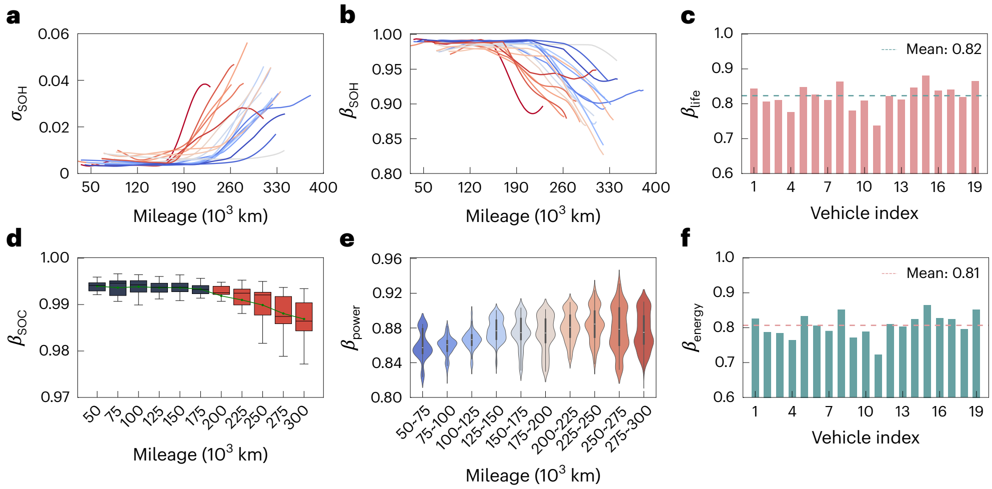

Fig. 5 | Impact of cell inconsistency on six battery-system performance metrics. **a**, Standard deviation of cell SOH values within each pack (σ_{SOH}) as a function of accumulated mileage for 19 electric cars; each curve represents one car. **b**, SOH utilization rate in each vehicle (β_{SOH}), constrained by the most aged cell. Averaging β_{SOH} at each car's end of life yields 0.938, corresponding to a 6.2% reduction in pack health attributable to cell imbalance. **c**, Utilization rate of battery lifetime (β_{life}), showing the extent of lifetime reduction due to early retirement of the most aged cell. The fleet average is 0.823, indicating a 17.7% shortening of pack lifetime. **d**, Utilization rate of battery SOC (β_{SOC}), which quantifies the impact of cell inconsistency on the pack's actual charged capacity. Red boxplots mark stages of pronounced decline. β_{SOC} generally remains above 0.98 overall, indicating a reduction generally below 2%. **e**, Utilization rate of battery power capability (β_{power}), limited by cell resistance inconsistencies. The fleet average is 0.871, corresponding to a 12.9% power loss. **f**, Utilization rate of battery energy resources (β_{energy}), determined by β_{SOC} and β_{life}. The fleet average is 0.807, meaning that 80.7% of the available energy resources are utilized over the operational lifetime of these EVs. For the boxplots in **d**, the centre line indicates the median, box bounds indicate the 25th and 75th percentiles, and whiskers extend to the most extreme non-outlier values within 1.5 times the interquartile range; outliers are not shown. For the violin plots in **e**, the width represents the distribution density of values within each mileage bin.

the increasing SOH inconsistency observed in Fig. 5a. A declining β_{SOH} signifies substantial performance degradation as the weakest cell acts as a bottleneck, particularly in series-connected battery packs. For example, the vehicle with the smallest β_{SOH} value of approximately 0.83 (light red curve) shows that only 83% of the pack's potential SOH is effectively utilized, with the remaining 17% lost due to cell inconsistency.

Cell inconsistency also reduces the lifetime of battery packs. To quantify this effect, we define β_{life} as the ratio of the equivalent full cycles (EFC) of the most aged cell to the average EFC of all cells in the pack. Analysis across the EV fleet (Fig. 5c) reveals an average β_{life} of 0.82, indicating that battery packs are retired approximately 18% earlier than the average lifespan of their individual cells. This early retirement occurs because the lifetime of a pack is primarily determined by its most degraded cell; once that cell reaches the end-of-life threshold, the entire pack is prematurely retired, causing substantial under-utilization of healthier cells. This premature retirement represents considerable resource inefficiency, an important concern given the global scale of EV adoption and the resources required for battery production. These findings emphasize the necessity for effective strategies to mitigate cell inconsistency, thereby extending battery lifetime and enhancing resource efficiency.

Inconsistencies in the SOC and SOH among individual battery cells can reduce the usable charge capacity of battery systems. To quantify this effect, we introduce the parameter β_{SOC}, defined as the ratio of the actual charged capacity to the maximum pack capacity if all cells were fully charged. These inconsistencies constrain the pack's ability to reach full charge, as charging protocols must be moderated to prevent overcharging cells with higher SOC or lower SOH. Consequently, the usable charge capacity decreases because the pack cannot fully exploit cells with lower SOC or healthier SOH. Figure 5d presents β_{SOC} values for EVs across varying mileage. Each boxplot represents EVs with available data at the corresponding mileage interval. The green curve illustrates the average β_{SOC} of different EVs, showing a gradual decline with increasing mileage. However, its overall impact remains substantially lower than those of β_{SOH} and β_{life}, typically staying below 2%. These results suggest that under the charging protocols and BMS balancing strategies represented in the analysed fleets, the practical impact of SOC imbalance on usable charged capacity appears modest.

Variations in cell resistance within battery packs notably affect their power capability. To quantify this, we define β_{power} as the ratio of the actual maximum power output to the theoretical maximum under homogeneous cell conditions. In series-connected battery packs, the maximum power is constrained by the cell exhibiting the highest resistance, which experiences the largest terminal voltage drop. The BMS limits this voltage drop to prevent over-discharge and overheating. Hence, β_{power} serves as a key indicator of power utilization efficiency. As illustrated in Fig. 5e, the fleet-average β_{power} remains relatively stable throughout the vehicle's lifespan, largely attributable to minor changes in resistance dispersion (Fig. 3h and Supplementary Fig. 6). On average, β_{power} ranges between 0.80 and 0.90, corresponding to approximately 10–20% reduction in power capability due to resistance heterogeneity.

To quantify the overall utilization rate of battery energy resources over the pack lifetime, we define the parameter β_{energy} as the product of β_{life} and the average value of β_{SOC}. Whereas β_{life} represents the long-term impact of SOH inconsistencies on battery lifespan, β_{SOC} captures short-term constraints on usable charge capacity per charging cycle (Supplementary Fig. 7). Thus, β_{energy} integrates both long-term and short-term utilization inefficiencies. As shown in Fig. 5f, β_{energy} ranges from 0.72 to 0.86 across the EV fleet, with an average of 0.81. This indicates that by the time of pack retirement, 19% of the available energy resources remain unused. Given the projected global Li-ion battery market valuation of US$400 billion by 2030[34], this under-utilization corresponds to an unrealized value of roughly US$76 billion. Importantly, β_{life} emerges as the dominant contributor to β_{energy}, as evidenced by the similarity between Fig. 5c,f. Therefore, improving the utilization of battery energy resources requires strategies that harmonize cell ageing rates and synchronize the end-of-life timing of individual cells to maximize battery usage and resource efficiency.

To broaden the scope of our analysis, we also examine electric buses equipped with LFP batteries. The results (Supplementary Figs. 8

and 9) are broadly consistent with those of electric passenger cars, although the average parameter values exhibit notable differences. At the end of life, the average β_{SOH} of the bus packs is 0.925, corresponding to a 7.5% loss of SOH. The mean β_{life} is 0.772, indicating a 22.8% reduction in lifetime, whereas β_{SOC} generally remains above 0.98, showing that SOC imbalance contributes less than 2% to overall under-utilization. The average β_{power} is 0.849, corresponding to a 15.1% decline in power capability. The mean utilization rate of battery energy resources (β_{energy}) in buses is 0.73, notably lower than the 0.81 observed in passenger cars. This difference probably arises from the greater difficulty of maintaining homogeneity in bus battery packs, which contain more cells (156 versus 95 in cars). The larger pack size intensifies spatial thermal gradients, accelerating differential ageing and amplifying cell-to-cell heterogeneity (Supplementary Fig. 10). In addition, the absence of explicit voltage balancing in these buses further exacerbates cell inconsistency (Supplementary Figs. 11–14). In the LFP bus packs, voltage dispersion increases substantially with ageing, reaching up to 300 mV in later stages (Supplementary Figs. 13–14). In contrast, the BMS in the NMC cars applies continuous passive balancing during charging, and the cell-voltage spread rarely exceeds 100 mV, even at advanced stages of ageing (Supplementary Figs. 11 and 12). This difference underscores the role of balancing control in suppressing the amplification of cell inconsistency. Unchecked inconsistency allows the most degraded cells to progressively diverge from the pack mean and dominate parameters such as β_{life} and β_{SOC}, ultimately reducing the utilization rate of battery energy resources (β_{energy}). Further details on automotive-grade cell variability, balancing and reconfiguration are provided in Supplementary Note 2.

Discussion

The multi-year fleet data enable examination of cell-level ageing and inconsistency over mileages up to 300,000 km in systems with different balancing strategies and operating conditions. In particular, the contrasting behaviours of the NMC (effectively balanced) and LFP (persistently unbalanced) systems show how balancing influences inconsistency evolution, with corresponding differences in performance, degradation and utilization. The comparison, based on large-scale real-world operational data, is consistent with prior expectations on the role of balancing and variability management.

Our results show several features of battery performance and degradation. SOH dispersion remains low over extended mileage ranges but increases beyond vehicle-specific ageing thresholds, with variation in onset and magnitude across vehicles. A fleet-average β_{SOH} of 0.94 at the end of life leaves approximately 6% of accessible pack SOH unavailable because of the weakest cells. Moreover, cell-level inconsistency also shortens pack lifetime: fleet-average β_{life} values of 0.82 for passenger cars and 0.77 for buses correspond to retirement around 18–23% earlier than the average lifetime of the constituent cells. SOC imbalance has a smaller effect on usable charge capacity, typically within 2%. Resistance heterogeneity reduces pack power capability, with β_{power} between 0.80 and 0.90 across the two vehicle types, corresponding to a 10–20% reduction in available pack power. Additionally, energy-resource utilization, β_{energy}, averages 0.81 for passenger cars and 0.73 for buses, leaving 19% and 27%, respectively, of available energy resources unrealized by the time of retirement.

Although the proposed NN normalization framework was assessed through complementary fleet-based and laboratory analyses, we note that complete disentanglement between intrinsic degradation mechanisms and all operational influences cannot be guaranteed in large-scale observational EV fleet studies. This limitation primarily arises from the absence of ground truth cell-level ageing trajectories under controlled real-world operation. The derived indicators should therefore be interpreted as operationally harmonized measures of long-term ageing evolution, rather than as isolated representations of intrinsic electrochemical ageing mechanisms.

In summary, cell-to-cell inconsistency imposes a fundamental limit on multiple performance metrics of battery packs. Unlocking additional utilization of EV batteries therefore probably requires mitigation strategies guided by quantitative measures of such inconsistencies. Reducing initial cell-to-cell variation through improved manufacturing and optimized cell grouping will help curb the amplification of deviations during ageing. In parallel, advanced balancing systems can suppress SOC divergence and differential ageing across cells, thereby improving pack utilization over time. Reconfigurable battery systems offer another potential route by using controllable power electronics around individual cells or cell groups to adapt pack operation to cell-level states and mitigate the consequences of inconsistency. Their benefits need to be weighed against increased hardware complexity, integration effort, parasitic losses and up-front costs. Importantly, the proposed metrics and fleet-derived ranges provide quantitative indicators for determining when and how these mitigation strategies should be deployed in practice.

Methods

Ageing indicators determination

To investigate how cell-to-cell variations translate into battery pack-level performance, we first require cell-level ageing indicators that are comparable across cells and over time on a like-for-like basis. In real-world fleet data, the apparent capacity and resistance inferred from voltage–current measurements are strongly influenced by operational conditions (for example, current, temperature and cumulative mileage), which complicates such comparisons. To address this, we develop a structured three-step framework to identify cell-level ageing indicators (capacity C and internal resistance R_0) and normalize them to a common reference condition. This framework comprises three steps.

In Step 1, the relationship between the OCV and SOC is established, and the ohmic resistance R_0 is independently determined. This is achieved by identifying wide-range, slow constant-current (CC) destination-charging processes (typically below 0.2C) for each studied EV and employing them to obtain the terminal voltage V and charging current I. The ohmic resistance R_0 is anchored using the current step transitions at the onset and termination of these charging events: a step change in current ΔI induces an instantaneous voltage jump ΔV that is dominated by the ohmic term, $\Delta V = R_0 \Delta I$. To mitigate the influence of measurement noise and potential sampling delay, R_0 is not computed from a single voltage difference; instead, a short window of voltage–current samples surrounding each transition is extracted and R_0 is estimated via local linear regression between ΔV and ΔI.

Partial OCV curves are then derived by subtracting the ohmic drop $R_0 I$ from the measured terminal voltage during CC charging. An example of the obtained OCV curves is shown in the middle panel of Fig. 2a. The partial OCV–SOC curves are subsequently extrapolated by fitting the left-hand side with a fourth-degree polynomial and the right-hand side with a linear function, as depicted in the right panel of Fig. 2a. Finally, the complete OCV–SOC curves are reconstructed using a tenth-degree polynomial fit (Supplementary Fig. 15).

In Step 2, building upon the OCV–SOC relationship and the ohmic resistance R_0 obtained in Step 1, parameter identification is performed using a first-order equivalent circuit model (ECM) in conjunction with particle swarm optimization, with R_0 treated as fixed. The ECM comprises an open-circuit voltage source OCV(SOC), the ohmic resistance R_0 and a single resistor–capacitor polarization branch characterized by R_p and C_p. The terminal voltage $V(t)$ of a cell is expressed as

$$V(t) = \mathrm{OCV}(\mathrm{SOC}(t)) + V_p(t) + R_0 I(t), \tag{1}$$

where t denotes time and $V_p(t)$ is the polarization voltage governed by

$$\mathring{V}_p(t) = -\frac{1}{R_p C_p} V_p(t) + \frac{1}{C_p} I(t). \tag{2}$$

 https://doi.org/10.1038/s41560-026-02131-5

With the accumulated charge during charging defined as $Q(t) = \int_0^t I(\tau)\,\mathrm{d}\tau$, the SOC evolves as

$$\mathrm{SOC}(t) = \mathrm{SOC}_0 + \frac{Q(t)}{C}, \tag{3}$$

where SOC_0 is the initial SOC at the beginning of the selected charging segment.

Parameter identification is restricted to quasi-steady portions of the aforementioned slow constant-current charging processes, sufficiently long after charging initiation such that the transient polarization dynamics have effectively converged. Under this excitation regime (that is, within the selected window $t \gg R_\mathrm{p}C_\mathrm{p}$), the polarization voltage approaches its steady-state value $V_\mathrm{p}(t) \approx R_\mathrm{p}I(t)$, and the terminal voltage can be approximated as

$$V(t) \approx \mathrm{OCV}(\mathrm{SOC}\,(t)) + R_\mathrm{p}I(t) + R_0 I(t). \tag{4}$$

Consequently, the effective free parameter set reduces to $\{R_\mathrm{p}, C, \mathrm{SOC}_0\}$. These parameters are estimated by minimizing the mean-squared error between the ECM-predicted terminal voltage $V(k)$ and its measured counterpart $V_\mathrm{meas}(k)$ over the selected charging window

$$J(\boldsymbol{\theta}) = \frac{1}{n}\sum_{k=1}^{n}\left[V_\mathrm{meas}(k) - V(k;\boldsymbol{\theta})\right]^2, \tag{5}$$

where $\boldsymbol{\theta} = [R_\mathrm{p}, C, \mathrm{SOC}_0]^\mathrm{T}$, k represents the discrete time index and n denotes the number of data samples.

The rationale for the excitation selection and the resulting local identifiability of the reduced parameter set are discussed in Supplementary Note 3.

In Step 3, the capacity and internal resistance estimates obtained in Step 2 for each battery cell are harmonized to facilitate systematic evaluation and meaningful comparison. Variations in ambient temperature and operational profiles inevitably introduce substantial uncertainties into the initial estimates of cell capacity and resistance. For a given mileage, each pair of identified capacity and resistance values represents battery ageing states only under the specific condition corresponding to the data used for parameter identification. Directly using these values, as shown in Fig. 2b, for battery diagnosis and analysis can therefore yield biased or erroneous conclusions.

To overcome this limitation, we introduce a neural-network (NN)-based approach in Step 3 to normalize the capacity and resistance values obtained in Step 2. The NN projects values measured under real-world operational conditions onto a standardized reference state. As an illustrative example, capacity values from Step 2 are treated as targets (outputs), while current, temperature and mileage serve as inputs. After training, the NN learns the mapping between capacity and these stress factors, thereby enabling the estimation of capacity under any combination of operational conditions. This framework not only harmonizes capacity values but also allows the influence of current, temperature and mileage to be systematically evaluated. A parallel strategy is applied to internal resistance, with the corresponding NN inputs shown in the left panel of Fig. 2c. Full details of the NN architectures, mathematical representation and training procedures are provided in Supplementary Note 3 and ref. 35.

In the implementation of these two NN models for capacity and internal resistance, a standardized reference condition is defined to ensure consistent normalization across heterogeneous operational contexts. The reference temperature is chosen as 27 °C, as it is close to the fleet-average operational temperature and thereby minimizes extrapolation during projection. In addition to temperature, the reference condition specifies an SOC of 50%, which lies near the mid-range of typical fleet operation and avoids boundary regions where strong nonlinearities or control constraints may dominate. Additional normalization settings are described in Supplementary Note 3, with implementation details provided in the accompanying code. All cell-level capacity and resistance estimates obtained in Step 2 are projected to this standardized reference condition, yielding the normalized trajectories shown in grey in the left and right panels of Fig. 2c. This normalization procedure ensures comparability of battery capacity and internal resistance values across different ageing states, EV operational environments and battery packs. In addition to cross validation on the real-world EV fleet dataset, the proposed framework is further validated through complementary fleet-based and laboratory analyses, including beginning-of-life reference measurements, BMS sensing perturbation tests, repeated neural-network training, OCV–SOC reconstruction and parameter identification across ageing states. The corresponding validation results are provided in Supplementary Note 4 and Supplementary Figs. 16–22. Fleet-level operating-stress distributions and additional pack-level case studies are shown in Supplementary Figs. 23–27.

Metrics to quantify pack-level effects of cell inconsistency

To quantify the impact of cell inconsistency on various pack-level performances, we introduce six metrics, as defined and explained as follows.

Standard deviation of cell SOH values, σ_SOH. To quantitatively assess cell-to-cell inconsistency within a battery pack, we use the standard deviation of the SOH values across all cells. Here the SOH of an individual cell is defined as the ratio of its current capacity to its nominal capacity (C_nom). Mathematically, the standard deviation of cell SOH values at a given cycle or mileage indexed by k is computed as:

$$\sigma_\mathrm{SOH}(k) = \sqrt{\frac{\sum_{i=1}^{N}\left(C_i(k) - \frac{1}{N}\sum_{j=1}^{N}C_j(k)\right)^2}{N C_\mathrm{nom}^2}} = \sqrt{\frac{\sum_{i=1}^{N}\left(\mathrm{SOH}_i(k) - \frac{1}{N}\sum_{j=1}^{N}\mathrm{SOH}_j(k)\right)^2}{N}}, \tag{6}$$

where C_i is the capacity of cell i estimated as detailed in the above subsection, and N denotes the total number of cells in the battery pack.

Utilization rate of battery SOH, β_SOH. The theoretical maximum pack capacity is defined as the capacity that would be achieved if all cells were homogeneous, each having the mean capacity of all cells. In a series-connected (single-parallel) pack, however, the usable capacity is limited by the cell with the lowest capacity, because all cells carry the same current during operation. As a result, even a small fraction of weaker cells can lead to substantial under-utilization of the available capacity. To quantitatively evaluate the extent of capacity under-utilization arising from cell-to-cell inconsistencies, we define the utilization rate of battery SOH, β_SOH, as the ratio of the minimum cell capacity to the mean cell capacity across the pack:

$$\beta_\mathrm{SOH}(k) = \frac{\min\{C_1(k), C_2(k), \cdots, C_N(k)\}}{\frac{1}{N}\sum_{i=1}^{N}C_i(k)} = \frac{\min\{\mathrm{SOH}_1(k), \mathrm{SOH}_2(k), \cdots, \mathrm{SOH}_N(k)\}}{\frac{1}{N}\sum_{i=1}^{N}\mathrm{SOH}_i(k)}. \tag{7}$$

Theoretically, β_SOH ranges between 0 and 1, where lower values reflect higher cell inconsistency and reduced effective capacity of the battery pack. Conversely, values approaching 1 indicate minimal inconsistency and better overall capacity utilization. The ideal scenario, $\beta_\mathrm{SOH}(k) = 1$, corresponds to perfect consistency where all cells exhibit identical SOH values at k.

Utilization rate of battery lifetime, β_life. While β_SOH captures transient inconsistencies in battery ageing, the utilization rate of battery lifetime,

β_{life}, specifically addresses the long-term implications of inconsistency related to replacement and retirement of battery packs. Mathematically, β_{life} is defined as:

$$\beta_{\mathrm{life}} = \frac{N \min\{\mathrm{EFC}_1, \mathrm{EFC}_2, \cdots, \mathrm{EFC}_N\}}{\sum_{i=1}^{N} \mathrm{EFC}_i}, \tag{8}$$

where EFC_i represents the EFC of cell i, evaluated at its defined end of life (EOL). The EFC is a measure used to quantify the total charge throughput of a battery in terms of complete charge–discharge cycles. It allows for the aggregation of partial cycles into an equivalent number of full cycles, providing a standardized metric for assessing battery usage and degradation. The EFC is defined as:

$$\mathrm{EFC} = \frac{\int_{t_0}^{t_f} |I(t)|\, dt}{2\, C_{\mathrm{nom}}}, \tag{9}$$

where t_0 and t_f denote the start and end of the measurement interval, respectively, and C_{nom} is the nominal cell capacity. For EV applications, the EOL criterion is typically set when the battery pack's SOH drops to 0.8. However, because the EVs studied in this work remain operational and have not yet reached this conventional threshold, we adopt a higher SOH threshold (0.85) as the EOL criterion for calculating EFC.

Similar to β_{SOH}, the lifetime utilization metric β_{life} theoretically ranges between 0 and 1. In practice, $\beta_{\mathrm{life}} = 0$ is unrealistic, as it would imply immediate cell failure with zero completed cycles. Lower values of β_{life} indicate substantial cell inconsistency and reduced pack lifetime, whereas higher values reflect uniform cell ageing and enhanced lifetime utilization. The ideal scenario, $\beta_{\mathrm{life}} = 1$, represents perfect consistency, where all cells age uniformly and simultaneously reach the EOL.

Utilization rate of battery SOC, β_{SOC}. In a battery pack, the SOC of individual cells is not always uniform due to variations in temperature, self-discharge, ageing and manufacturing tolerances. This SOC imbalance can lead to premature charge/discharge cut-offs, thereby reducing the usable charge of the pack during operation. To quantify this loss, we define the metric β_{SOC}, which captures the degree to which SOC imbalance limits the pack's ability to utilize its available charge at a given moment

$$\beta_{\mathrm{SOC}}(t) = 1 - \frac{\sum_{i=1}^{N} (\mathrm{SOC}_{\max}(t) - \mathrm{SOC}_i(t)) \times \mathrm{SOH}_i(k)}{\sum_{i=1}^{N} \mathrm{SOH}_i(k)}, \tag{10}$$

$$\mathrm{SOC}_{\max}(t) = \max\{\mathrm{SOC}_1(t), \mathrm{SOC}_2(t), \cdots, \mathrm{SOC}_N(t)\}, \tag{11}$$

where $\mathrm{SOC}_{\max}(t)$ represents the maximum SOC among all cells in the pack at time t. The normalization by SOH ensures that charge imbalance is properly weighted according to the capacity of each cell. In our implementation, t in equation (11) is specified as the time corresponding to the end of charge for battery packs.

Here $\beta_{\mathrm{SOC}}(t) = 1$ corresponds to the ideal case where all cells are perfectly balanced in SOC, leading to the maximum usable charge. Conversely, $\beta_{\mathrm{SOC}}(t) \approx 0$ would represent a theoretical extreme in which only one cell stores full charge (SOC = 100%) while all others are completely discharged (SOC = 0%), resulting in effectively no usable pack-level charge. Lower β_{SOC} values indicate greater SOC imbalance and reduced charge utilization, while values closer to 1 reflect well-balanced operation.

Utilization rate of battery power capability, β_{power}. To quantitatively assess how internal resistance inconsistency among cells impacts the battery pack's overall power capability (P_{pack}), we introduce the metric β_{power}, defined as

$$\beta_{\mathrm{power}}(t) = \frac{P_{\mathrm{pack}}}{\sum_{i=1}^{N} P_{\mathrm{cell},i}}, \tag{12}$$

where P_{pack} and $P_{\mathrm{cell},i}$ represent the maximum available power from the battery pack and individual cell i, respectively. We assume P_{pack} and $P_{\mathrm{cell},i}$ are constant during the prediction horizon, consistent with prior literature[36,37].

Following[36], the cell-level maximum available power $P_{\mathrm{cell},i}$ at time t is calculated as

$$P_{\mathrm{cell},i} = I_{\max,i} \left[V(t) + R_0 \left(I_{\max,i} - I(t) \right) \right], \tag{13}$$

$$I_{\max,i} = \frac{\Delta V_{\mathrm{lim}}(t) + R_0 I(t) + V_{\mathrm{p}}(t) \left(1 - e^{-\frac{\Delta t}{R_{\mathrm{p}} C_{\mathrm{p}}}} \right)}{R_0 + R_{\mathrm{p}} \left(1 - e^{-\frac{\Delta t}{R_{\mathrm{p}} C_{\mathrm{p}}}} \right)}, \tag{14}$$

where Δt denotes the prediction horizon within which the power capability is evaluated. $I_{\max,i}$ represents the maximum permissible constant current of cell i over the prediction interval $[t, t + \Delta t]$. ΔV_{lim} represents the maximum voltage margin constrained by the predefined cut-off voltage $V_{\max}$, namely $\Delta V_{\mathrm{lim}}(t) = V_{\max} - V(t)$. After the ohmic resistance R_0 and the polarization resistance R_{p} are identified in the above subsection, short transient segments containing observable current variations are further utilized to estimate the time constant $\tau_{\mathrm{p}} = R_{\mathrm{p}} C_{\mathrm{p}}$ associated with the resistor–capacitor branch. This supplementary estimation is used for power capability evaluation.

At the pack level, P_{pack} can be similarly determined as

$$P_{\mathrm{pack}} = I_{\max} \left[V_{\mathrm{pack}}(t) + R_{0,\mathrm{pack}} \left(I_{\max} - I_{\mathrm{pack}}(t) \right) \right], \tag{15}$$

where $I_{\mathrm{pack}}(t)$ and $V_{\mathrm{pack}}(t)$ are the measured current and voltage of the battery pack at time t. The maximum allowable pack-level constant-current $I_{\max}$, ensuring all cell-level constraints are respected, is defined by:

$$I_{\max} = \min\{I_{\max,1}, I_{\max,2}, \cdots, I_{\max,N}\}. \tag{16}$$

Combining equations (13)–(16) into (12), we obtain the power utilization metric β_{power}. Lower values of β_{power} indicate higher internal resistance inconsistency among cells, leading to diminished pack-level power performance, whereas higher values reflect enhanced power capability.

Utilization rate of battery energy resources, β_{energy}. To evaluate how effectively a battery pack's electrochemical energy resources are utilized over its operational lifetime, we define the metric β_{energy}, referred to as the utilization rate of battery energy resources. This metric quantifies the fraction of the nominal energy throughput that is actually realized before pack retirement, accounting for both premature ageing and cell-level SOC imbalance. Formally, β_{energy} is defined as the product of the lifetime utilization rate β_{life} and the averaged SOC utilization rate $\langle \beta_{\mathrm{SOC}} \rangle$, namely

$$\beta_{\mathrm{energy}} = \beta_{\mathrm{life}} \langle \beta_{\mathrm{SOC}} \rangle, \tag{17}$$

where $\langle \beta_{\mathrm{SOC}} \rangle$ denotes the average value of β_{SOC}, as defined in equation (10), over the battery pack's entire lifetime. β_{SOC} is a scalar parameter and represents the degree to which the SOC imbalance constrains the pack's ability to use its available charge at a given moment.

The resulting metric reflects the compounded efficiency with which the battery pack's designed energy-handling capability is exploited over its entire service life. Lower values of β_{energy} indicate that a substantial portion of the energy resources remains underutilized due to internal inconsistencies, while values approaching unity correspond to near-optimal resource efficiency.

Data availability

The data supporting the main analyses and figures are available via GitHub at https://github.com/Rico-dicp/Ev-battery-cell-to-cell-inconsistency. Source data are provided with this paper.

Code availability

The code supporting the data processing, analysis and figure generation is publicly available via GitHub at https://github.com/Rico-dicp/Ev-battery-cell-to-cell-inconsistency.

References

1. Hou, J. et al. Battery inconsistency evaluation based on hierarchical weight fusion and fuzzy comprehensive evaluation method. *J. Energy Storage* **84**, 110878 (2024).
2. Duan, B., Li, Z., Gu, P., Zhou, Z. & Zhang, C. Evaluation of battery inconsistency based on information entropy. *J. Energy Storage* **16**, 160–166 (2018).
3. Cui, Z., Cui, N., Rao, J., Li, C. & Zhang, C. Current distribution estimation of parallel-connected batteries for inconsistency diagnosis using long short-term memory networks. *IEEE Trans. Transp. Electrif.* **8**, 1013–1025 (2021).
4. Zhao, D. et al. Health condition assessment of satellite Li-ion battery pack considering battery inconsistency and pack performance indicators. *J. Energy Storage* **60**, 106604 (2023).
5. Müller, V., Scurtu, R.-G., Memm, M., Danzer, M. A. & Wohlfahrt-Mehrens, M. Study of the influence of mechanical pressure on the performance and aging of lithium-ion battery cells. *J. Power Sources* **440**, 227148 (2019).
6. Severson, K. A. et al. Data-driven prediction of battery cycle life before capacity degradation. *Nat. Energy* **4**, 383–391 (2019).
7. Baumhöfer, T., Brühl, M., Rothgang, S. & Sauer, D. U. Production caused variation in capacity aging trend and correlation to initial cell performance. *J. Power Sources* **247**, 332–338 (2014).
8. Li, W. et al. One-shot battery degradation trajectory prediction with deep learning. *J. Power Sources* **506**, 230024 (2021).
9. Tang, X. et al. Detecting abnormality of battery lifetime from first-cycle data using few-shot learning. *Adv. Sci.* **11**, 2305315 (2024).
10. Che, Y. et al. Lifetime and aging degradation prognostics for lithium-ion battery packs based on a cell to pack method. *Chin. J. Mech. Eng.* **35**, 1–16 (2022).
11. Hoekstra, F. S. J., Bergveld, H. J. & Donkers, M. Optimal control of active cell balancing: extending the range and useful lifetime of a battery pack. *IEEE Trans. Control Syst. Technol.* **30**, 2759–2766 (2022).
12. Xie, Y. et al. Improving battery thermal behavior and consistency by optimizing structure and working parameter. *Appl. Therm. Eng.* **196**, 117281 (2021).
13. Fang, W., Chen, H. & Zhou, F. Fault diagnosis for cell voltage inconsistency of a battery pack in electric vehicles based on real-world driving data. *Comput. Electr. Eng.* **102**, 108095 (2022).
14. Che, Y. et al. Joint estimation of inconsistency and state of health for series battery packs. *Automot. Innovation* **4**, 103–116 (2021).
15. Feng, X., Zhang, X. & Xiang, Y. An inconsistency assessment method for backup battery packs based on time-series clustering. *J. Energy Storage* **31**, 101666 (2020).
16. Jeng, S.-L. & Chieng, W.-H. Evaluation of cell inconsistency in lithium-ion battery pack using the autoencoder network model. *IEEE Trans. Ind. Inf.* **19**, 6337–6348 (2022).
17. Tian, J. et al. Feature fusion-based inconsistency evaluation for battery pack: improved gaussian mixture model. *IEEE Trans. Intell. Transp. Syst.* **24**, 446–458 (2022).
18. Tian, J., Wang, Y., Liu, C. & Chen, Z. Consistency evaluation and cluster analysis for lithium-ion battery pack in electric vehicles. *Energy* **194**, 116944 (2020).
19. Qiu, Y., Cao, W., Peng, P. & Jiang, F. A novel entropy-based fault diagnosis and inconsistency evaluation approach for lithium-ion battery energy storage systems. *J. Energy Storage* **41**, 102852 (2021).
20. Ouyang, Q., Ghaeminezhad, N., Li, Y., Wik, T. & Zou, C. A unified model for active battery equalization systems. *IEEE Trans. Control Syst. Technol.* **33**, 685–699 (2025).
21. Qu, F. et al. Systematic overview of active battery equalization structures: mathematical modeling and performance evaluation. *IEEE Trans. Energy Convers.* **37**, 1685–1703 (2022).
22. Han, W., Wik, T., Kersten, A., Dong, G. & Zou, C. Next-generation battery management systems: dynamic reconfiguration. *IEEE Ind. Electron. Mag.* **14**, 20–31 (2020).
23. Ouyang, Q., Han, W., Zou, C., Xu, G. & Wang, Z. Cell balancing control for lithium-ion battery packs: a hierarchical optimal approach. *IEEE Trans. Ind. Inf.* **16**, 5065–5075 (2020).
24. Ouyang, Q. et al. Mathematical modeling for reconfigurable battery systems with parallel–series connections. *IEEE Trans. Control Syst. Technol.* **34**, 186–202 (2026).
25. *Part 3: Communication Protocol and Data Format, Technical Specifications of Remote Service and Management System for Electric Vehicles* (General Administration of Quality Supervision, Inspection and Quarantine of the People's Republic of China and Standardization Administration of China, 2016).
26. Zhao, Y., Wang, Z., Shen, Z.-J. M. & Sun, F. Assessment of battery utilization and energy consumption in the large-scale development of urban electric vehicles. *Proc. Natl Acad. Sci. USA* **118**, e2017318118 (2021).
27. Škegro, A., Wik, T., Bijlenga, B., Bessman, A. & Zou, C. System-level assessment of dynamic reconfiguration for lifetime and cost outcomes in electric vehicle battery packs. *Nat. Commun.* **17**, 5980 (2026).
28. Liu, H. et al. Multi-modal framework for battery state of health evaluation using open-source electric vehicle data. *Nat. Commun.* **16**, 1137 (2025).
29. He, Z. et al. An estimation framework for battery pack state of health based on real vehicle charging and discharging features. *J. Power Sources* **631**, 236235 (2025).
30. Pozzato, G. et al. Analysis and key findings from real-world electric vehicle field data. *Joule* **7**, 2035–2053 (2023).
31. Lam, V. N. et al. A decade of insights: delving into calendar aging trends and implications. *Joule* **9**, 101796 (2025).
32. Zhou, L., Zhao, Y., Li, D. & Wang, Z. State-of-health estimation for $LiFePO_4$ battery system on real-world electric vehicles considering aging stage. *IEEE Trans. Transp. Electrif.* **8**, 1724–1733 (2021).
33. Liu, K., Tang, X., Teodorescu, R., Gao, F. & Meng, J. Future ageing trajectory prediction for lithium-ion battery considering the knee point effect. *IEEE Trans. Energy Convers.* **37**, 1282–1291 (2021).
34. Fleischmann, J. et al. *Battery 2030: Resilient, Sustainable, and Circular* (McKinsey & Company, 2023).
35. Zhang, Y. *Data-Driven Battery Aging Diagnostics and Lifetime Extension*. PhD thesis, Chalmers Univ. of Technology (2024); https://research.chalmers.se/en/publication/543724
36. Fridholm, B., Wik, T., Kuusisto, H. & Klintberg, A. Estimating power capability of aged lithium-ion batteries in presence of communication delays. *J. Power Sources* **383**, 24–33 (2018).
37. Zou, C. et al. Power capability prediction for lithium-ion batteries using economic nonlinear model predictive control. *J. Power Sources* **396**, 580–589 (2018).

Acknowledgements

We acknowledge the National Academic Infrastructure for Supercomputing in Sweden (NAISS) at Chalmers University of Technology for providing computational resources.

Author contributions

C.Z., L.Z. and X.B. conceptualized the study and developed the methodology. Y.Z. contributed to the methodology for experimental data acquisition and neural-network training. Z.M. contributed to the parameter identification calculations. L.Z. performed the experiments and simulations under the guidance of C.Z. and X.B. L.Z., X.B. and C.Z. conducted the main data analysis, validation and visualization, with input from Z.C. and Z.M. on result interpretation and practical implications. C.Z. and Z.C. supervised the study, acquired funding and conducted project administration. Z.W., C.Z. and Z.C. provided resources, including data and the testing environment. C.Z., L.Z. and X.B. jointly wrote the original draft. All authors contributed to reviewing and editing the paper and approved the submitted version.

Funding

This work was supported by the Swedish Research Council (grant number 2023-04314), the Strategic Priority Research Program of the Chinese Academy of Sciences (grant number XDB0600400), the National Natural Science Foundation of China (grant number U21A20170), the Swedish Energy Agency within the Vehicle Strategic Research and Innovation Program (grant number P2023-00611) and the European Union's Horizon Europe programme under the Marie Skłodowska-Curie Actions (grant number 101131278). The computational resources provided by the National Academic Infrastructure for Supercomputing in Sweden (NAISS) were partially funded by the Swedish Research Council (grant number 2022-06725). Open access funding was provided by Chalmers University of Technology. Open access funding provided by Chalmers University of Technology.

Competing interests

The authors declare no competing interests.

Additional information

Supplementary information The online version contains supplementary material available at https://doi.org/10.1038/s41560-026-02131-5.

Correspondence and requests for materials should be addressed to Zhongwei Chen or Changfu Zou.

Peer review information *Nature Energy* thanks Woongchul Choi, Karimi Reza and the other, anonymous, reviewer(s) for their contribution to the peer review of this work.